Mech Time-Depend Mater (2012) 16:251–274
DOI 10.1007/s11043-011-9155-8

Constant strain rate experiments and constitutive modeling for a class of bitumen

Kommidi Santosh Reddy · S. Umakanthan · J. Murali Krishnan

Received: 18 December 2010 / Accepted: 16 September 2011 / Published online: 27 October 2011

Abstract The mechanical properties of bitumen vary with the nature of the crude source and the processing methods employed. To understand the role of the processing conditions played in the mechanical properties, bitumen samples derived from the same crude source but processed differently (blown and blended) are investigated. The samples are subjected to constant strain rate experiments in a parallel plate rheometer. The torque applied to realize the prescribed angular velocity for the top plate and the normal force applied to maintain the gap between the top and bottom plate are measured. It is found that when the top plate is held stationary, the time taken by the torque to be reduced by a certain percentage of its maximum value is different from the time taken by the normal force to decrease by the same percentage of its maximum value. Further, the time at which the maximum torque occurs is different from the time at which the maximum normal force occurs. Since the existing constitutive relations for bitumen cannot capture the difference in the relaxation times for the torque and normal force, a new rate type constitutive model, incorporating this response, is proposed. Although the blended and blown bitumen samples used in this study correspond to the same grade, the mechanical responses of the two samples are not the same. This is also reflected in the difference in the values of the material parameters in the model proposed. The differences in the mechanical properties between the differently processed bitumen samples increase further with aging. This has implications for the long-term performance of the pavement.

Keywords Bitumen · PDA Pitch · Aging · Constant strain rate · Blended · Air blown · Rate type constitutive relation

K.S. Reddy · S. Umakanthan · J.M. Krishnan (✉)
Department of Civil Engineering, Indian Institute of Technology Madras, Madras, India
e-mail: jmk@iitm.ac.in

K.S. Reddy
e-mail: santoshko05@gmail.com

S. Umakanthan
e-mail: saran@iitm.ac.in

1 Introduction

The use of bitumen as a binder for highway and runway pavement construction is well known (Krishnan and Rajagopal 2003). Taking into account the considerable financial costs in a road and runway project where bitumen is used, the necessity to develop fundamental understanding of the mechanical behavior of the material cannot be overemphasized.

Developing an understanding of bitumen is hindered by several complexities. Krishnan and Rajagopal (2005) classify the main stumbling blocks toward rigorous characterization of bitumen under three heads. The first one is related to the multi-constituent nature of bitumen, the second one is related to the development of internal structure in bitumen and its evolution at rest and the third is related to the transitory nature of bitumen during temperature change. Apart from these stumbling blocks, the response of bitumen seems to depend on the nature of the petroleum crude used and the subsequent processing methods followed to produce a binder of specific grade or specification.

Bitumen is normally processed by two different methods, and the production process is adjusted so that bitumen with specific properties is produced. The final property required depends on the technical parameters such as viscosity at a specific temperature (ASTM D3381 2009) or performance required in the field condition, quantified through some linear viscoelastic parameters (ASTM D6373 2007).

In the first process, the residue from the vacuum fractionation tower, consisting of a less viscous material, is subjected to hot air blowing such that the final product has the required consistency. In the second process, the vacuum residue is contacted with propane to extract oils collectively known as deasphalted oil. The precipitate is called propane deasphalted (PDA) pitch (Newman 1976). This PDA pitch is a very hard material, with the consistency of a rock with a penetration value around 0–5 measured as per ASTM D5 (2006) and is used as a blending component for bitumen production. The production of bitumen for paving purposes is carried out by blending the extract from the residuum stream with the PDA pitch (Rakow 2003). Depending on the properties required, the appropriate proportions of PDA pitch and extract are determined. Normally these proportions vary from 80:20 to 90:10 (PDA pitch : heavy extract) depending on the grade processed. Typically, the choice of these proportions is based on assuming the classical Arrhenius model (Hatschek 1928) for mixing. It is interesting to point out here that during the air blowing process bitumen is processed from a soft consistency material (vacuum residue); in the blending process, it is processed from a hard consistency material (PDA pitch). Needless to say that the rheological properties are different, though bitumen processed by these two methods will have the same specification parameter, namely the viscosity at a specific temperature (Rajan et al. 2008).

Due to the complexity related to characterizing bitumen experimentally and analytically, most of the studies in bituminous pavement engineering have mainly focused on the linear viscoelastic response of the material. In all these studies, either an integral model or a rate-type model is used. The main emphasis in all these studies is more on identifying the material parameters which can be related to the expected pavement performance in terms of rutting or cracking. These constitutive models, used to describe the linear viscoelastic response of bitumen, use a linearized strain measure and hence characterize the material only when the rotations and change in length of the material filaments are small. When the strains are large (say greater than 1 percent) one cannot use linearized strain and hence these models. In fact, the strains observed during rutting or cracking are considerably large. Consequently, we investigate here the response of the bitumen subject to 25 percent shear strain and find that significant normal stresses develop, with the magnitude, of course, depending on the shear rate. It is well known that theories based on linearized strain measures cannot predict

the development of these normal stresses. Hence, we require non-linear models of the type developed here.

Lethersich (1942) is credited with using for the first time Burgers' model for describing the response of bitumen, and one can find details related to earlier attempts in the review article of Krishnan and Rajagopal (2003). Motivated by the experiments of Lethersich (1942) on bitumen, Fröhlich and Sack (1946) developed rate-type models for the viscoelastic response of dispersions. Oldroyd (1950) used the constitutive equations of an incompressible elasticoviscous liquid derived by Fröhlich and Sack (1946) and developed a refined version of this model by using appropriate frame-invariant time derivatives. van der Poel (1958) used the method of Fröhlich and Sack (1946) to calculate the viscosity and shear modulus of bitumen and in this context, and it is worthwhile to quote Oldroyd's rejoinder to this work on bitumen as follows: "*I am interested to know if Dr. van der Poel has a simple argument to justify in principle the use of the perturbation method of Fröhlich and Sack for values of the concentration which are not infinitesimal*" (van der Poel 1961).

Dobson (1969) developed master curves for the complex shear modulus as a function of frequency. Dickinson and Witt (1969) and Dickinson (1970) investigated the linear viscoelastic behavior of thin films of bitumen in tension and compression and loading in a direction normal to the plane. Jongepier and Kuilman (1970) investigated the frequency dependence of the dynamic moduli and concluded that one can describe it by Gaussian distributions of the log of the relaxation time. Attané et al. (1984) collected steady-state and transient shear stress and normal stress data for different types of asphalt and indicated that one could use a time–temperature superposition even in the non-linear regime. The use of the time–temperature superposition principle to predict the rheological response of bitumen over several decades of temperature is subject to considerable controversy, and one can find details related to this in the review article by Lesueur (2009). Hraiki (1975) proposed a viscoplastic model consisting of many groups of Newtonian and Saint-Venant elements in parallel. A bimodal description for the viscoelastic properties of asphalt is given in the significant work carried out by Lesueur et al. (1996). These authors also demonstrated that the time–temperature superposition principle failed at high temperature specifically for asphalt having a high asphaltene content and high crystalline content. However, Cheung and Cebon (1997) proposed that the temperature dependence of the bitumen tested by them was found to follow the Arrhenius relationship above the glass transition temperature and the WLF equation was found to be valid at higher temperature. Cheung and Cebon (1997) proposed different models for different temperature regimes; below the glass transition temperature, the Eyring plasticity model was found to hold and a power law to model the creeping behavior at higher stress levels was found for higher temperatures. Stastna and Zanzotto (1999) investigated the use of a fractional model for bitumen to describe the mechanical and dielectric transitions. Recently Ossa et al. (2005) used a modified Cross model to capture the monotonic response under constant strain rate and creep behavior. They assumed that the viscosity could be described as a function of the strain rate. Ossa et al. (2005) extended this model to a fully three-dimensional loading using a von Mises criterion. Krishnan and Rajagopal (2005) used a thermodynamic framework to derive a constitutive model for bitumen. The framework proposed by them takes into account the fact the stress-free configuration of the material can evolve with time. Assuming that bitumen can be modeled as a mixture of amorphous and crystalline material, they used two relaxation times in their model. Vijay et al. (2008) used a first order kinetic equation along with the non-linear rheological model of White–Metzner and used steady shear and oscillatory shear data to model and predict the response of bitumen in the temperature range of 20–60°C. It is also interesting to point out here some of the recent work of Wekumbura et al. (2005, 2007) for polymer modified

binders wherein the stress overshoot during steady shear was related to the network structure of the material. Filograna et al. (2009) described a three-dimensional non-linear generalization of the standard three-parameter model of one-dimensional classical viscoelasticity and showed that these kinds of model could be used to describe the response of bitumen.

The complexity of the constitution of bitumen results in the material showing a mechanical response different from many other viscoelastic polymers. Such a mechanical response includes for instance, shear stress and normal stress difference overshoot during steady shear experiments, and one has a difference in the time taken for the shear stress and normal stress difference to reduce by say 80 percent of its maximum value during constant strain experiments and the possibility of a lag between shear stress and normal stress difference during oscillatory shear. Chockalingam et al. (2010) showed that stress overshoot cannot be modeled using explicit constitutive relations of the form

$$\overset{\nabla}{\boldsymbol{\tau}} = \lambda \boldsymbol{\tau} + \eta \mathbf{d}, \tag{1}$$

where λ and η are material response functions which depend on the principal invariants of $\mathbf{d}$, $\mathbf{d}$ is the symmetric part of the Eulerian velocity gradient, $\boldsymbol{\tau}$ is that part of the Cauchy stress, which is determined by the deformation history, and $\overset{\nabla}{\boldsymbol{\tau}}$ denotes a frame-invariant material time derivative of the stress. Chockalingam et al. (2010) also developed an implicit constitutive relation using the framework proposed in Rajagopal and Srinivasa (2011) that is able to capture the stress overshoot. Rajagopal and co-workers realized the need for such implicit models to capture the response of real-life materials and are developing a general framework for generating such models (see Rajagopal 2006, 2007; Rajagopal and Srinivasa 2008, 2009).

In this article, we develop a model which shows different relaxation times for the normal and shear stress. Here again we found that an explicit constitutive equation of the form of (1) will always have the same relaxation times for the normal and shear stresses. Hence, an implicit constitutive relation is developed. Details are presented in Sect. 3. Before that, in Sect. 2, the details of the experiments conducted and salient observations from the experiments are presented. In the final section we discuss the corroboration between the experimental results and the predictions of the model.

2 Experimental investigations

This investigation focuses on characterizing the rheological properties of blended and air blown bitumen processed from the same crude source. The processing conditions of the bitumen prepared by the air blowing and blending processes were such that the final bitumen met the VG30 standards of BIS (2006). Arab mix crude source was used for preparing the bitumen by the two processes. A ratio of 90:10 (PDA pitch:Heavy extract) was used in the preparation of bitumen by the blending process. The pertinent properties of air blown and blended asphalt used for the investigation are listed in Table 1. In addition, the PDA pitch was also tested to understand its influence on the mechanical behavior of blended bitumen. Each material was subjected to two aging conditions. The first aging condition corresponds to short-term aging. This aging simulates in the laboratory the approximate change in properties of bitumen during hot mixing around a temperature of 150°C. The residue resulting from this aging procedure is approximately equal to the condition of the binder in the pavement immediately after construction. In this investigation, the short-term aging was performed according to the procedure specified in the ASTM D2872 (2004). The

Table 1 Properties of materials as per IS: 73, 2006

Specification	Air blown Asphalt	Blended Asphalt
Absolute viscosity at 60 (°), Poises	3920	3250
Kinematic viscosity at 135 (°C), cSt	534	580
Penetration at 25 (°C), 100 g, 5 s, 0.1 mm	65	69
Softening point (R&B), (°C)	52	49
Viscosity ratio at 60°C (Short-term aged to unaged)	2	2.4

second aging condition corresponds to long-term aging. This test procedure uses the residue resulting from short-term aging and ages it further; it then results in a material similar to that subjected to oxidative aging during pavement service. Typically, this aging simulates approximately the condition of the material 7–10 years in service. Here this long-term aging was performed as per the guidelines specified in ASTM D6521 (2008).

Each of the three different materials—bitumen prepared by the two different processes and the PDA pitch—were subjected to two aging conditions—short-term and long-term aging—resulting in six different samples. In addition to this, three unaged samples, corresponding to each of these three different materials, were tested.

All experiments were conducted using an Anton–Paar dynamic shear rheometer, model MCR301. A parallel plate system with plates of 8 mm diameter was used. The gap between the parallel plates was maintained at 1 mm. All the tests were conducted in isothermal conditions at 26°C. This test temperature was chosen after several trials so as to ensure that all the nine materials (air blown and blended bitumen and PDA pitch under unaged, short-term aged and long-term aged condition) could be subjected to the same displacement field without exceeding the torque and normal force limits of the equipment. All the samples were conditioned and tested as per the appropriate ASTM test protocol ASTM D7552 (2009) related to the dynamic shear rheometer.

All the nine samples were subjected to the same protocol, in which the bottom plate was held fixed and the top plate was rotated in the clockwise direction for t_o seconds, then held stationary for 2 seconds, and then rotated in the counterclockwise direction for t_o seconds and again held stationary for 2 seconds. The duration up to which the top plate was rotated, t_o, depends on the targeted angular displacement at the periphery of the plate and the maximum angular velocity which it was subjected to. Experiments were performed for two different maximum angular velocities: 0.25 rad/s and 0.625 rad/s. If the angular velocity was below a particular value, repeatable measurements of the normal force could not be obtained as it was below the resolution limit of the load cell. On the other hand, if the angular velocity was above a particular limit, the normal force developed exceeded the capacity of the load cell. It was also found that these critical lower and upper limits for the angular velocity depended on the type of sample being tested. The angular velocity chosen was found to be optimal given all the above constraints. The targeted angular displacement at the periphery of the cylinder was 0.25 mm. This angular displacement corresponds to a shear strain of 25 percent. This cycle of clockwise rotation, being held stationary, undergoing counterclockwise rotation, and being held stationary, was repeated thrice.

One important aspect related to the conduct of these experiments is the data acquisition rate. To precisely capture the response of the material as the angular velocity is varied, different trial experiments were conducted before choosing a correct measuring point duration. For the angular velocity of 0.25 rad/s, 50 data points were collected during the period when

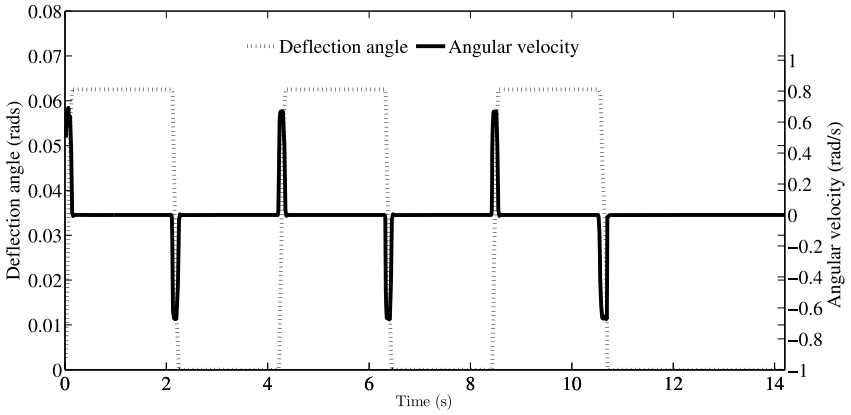

Fig. 1 Variation of deflection angle and angular velocity with time

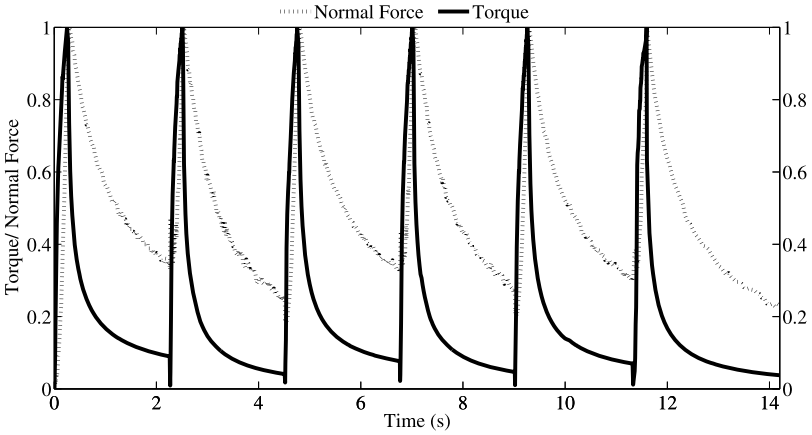

Fig. 2 Variation of normalized torque and normal force with time for PAV aged air blown sample tested at a maximum angular velocity of 0.25 rad/sec for three cycles

the top plate was rotated with a measuring point duration of 0.005 s. For the angular velocity of 0.625 rad/s, 25 data points were collected during the period when the top plate was rotated with a measuring point duration of 0.004 s. For the time in which the plate was held stationary, 100 data points were collected with a measuring point duration of 0.02 s.

The actual variation of the deflection angle and angular velocity in a typical experiment is shown in Fig. 1 for the case when the maximum angular velocity that the sample is subjected to is 0.625 rad/s. During these experiments, the torque applied to realize the prescribed angular velocity for the top plate and the normal force applied to maintain the gap between the top and bottom plate were measured.

Figure 2 plots the variation of the normalized torque and normal force for PAV aged air blown sample tested at an angular velocity of 0.25 rad/s. The normalized torque (normal force) is obtained by dividing the torque (normal force) applied at time t by the maximum torque (normal force) applied in this protocol. For easy comparison, the negative torque obtained during counterclockwise rotation is also plotted as positive. From this figure we can

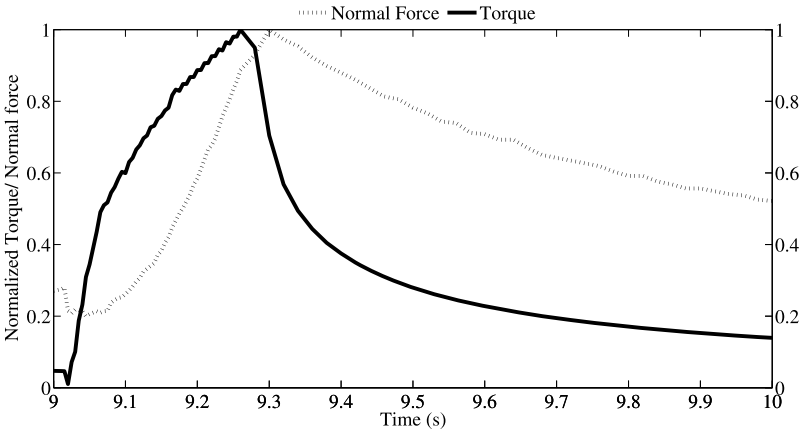

Fig. 3 Variation of the normalized torque and normal force with time for PAV aged air blown sample tested at a maximum angular velocity of 0.25 rad/sec for the third cycle

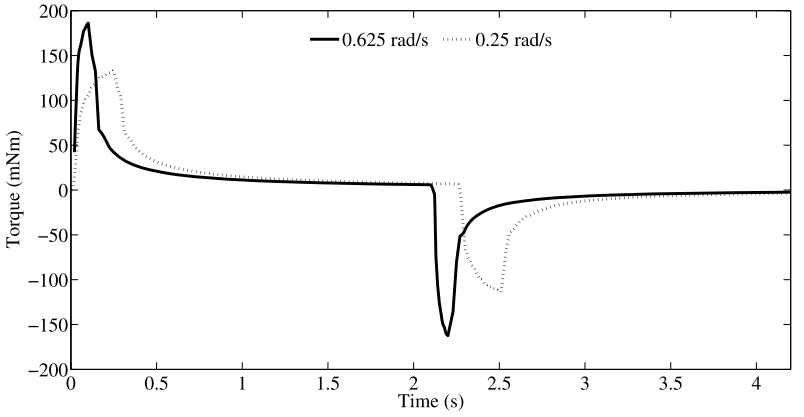

Fig. 4 Variation of torque with time for PAV aged PDA pitch for different angular velocities

infer that the time taken by the torque to be reduced by, say, 50 percent from its maximum value is different from the time taken by the normal force to decrease by the same percentage. In Fig. 3 we zoom in on the third cycle of the results presented in Fig. 2. It can be seen from this figure that the time at which the maximum torque needs to be applied is different from the time at which the maximum normal force occurs. This happens even in the first cycle. These observations suggest that the relaxation times for the shear and normal stresses are different and this is an important characteristic that the developed model should possess. Even though we show this only for the long-term aged air blown bitumen sample, the same observations hold for other samples too.

While in Fig. 4 the variation of the torque with time for two different angular velocities is portrayed, in Fig. 5 we plot the variation of the normal force for the same two angular velocities. It is clear from these figures that the magnitude of the torque and normal force

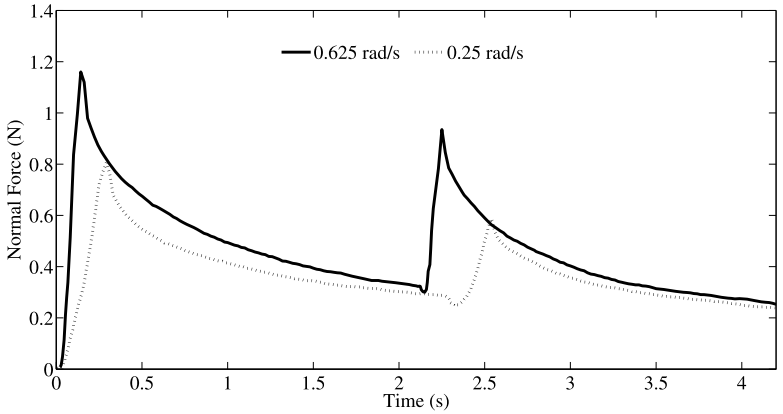

Fig. 5 Variation of normal force with time for PAV aged PDA pitch for different angular velocities

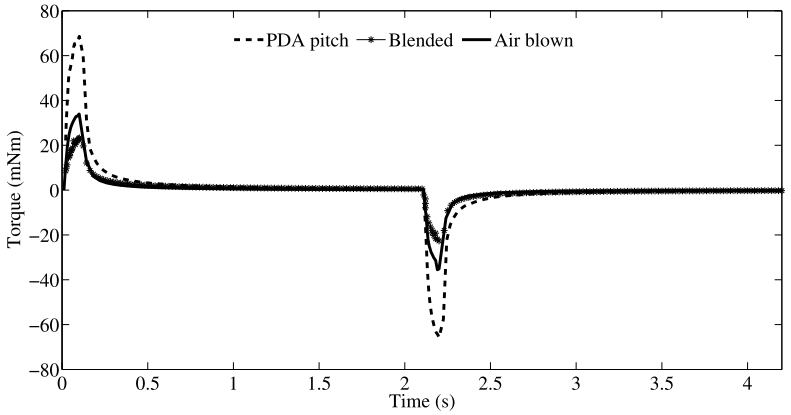

Fig. 6 Variation of torque with time for unaged specimens tested at a maximum angular velocity of 0.625 rad/s

depends on the angular velocity of the top plate. This suggests that the stress depends on the velocity gradient.

It can be seen from Fig. 6 that the torque required to realize a given deformation history is higher for PDA pitch in comparison to air blown and blended bitumen. Even though 90 percent of the blended bitumen is PDA pitch, it requires significantly much less torque than PDA pitch to realize the given deformation history. Similarly, it can be seen from Fig. 7 that the time taken by the torque to decrease to say 20 percent of the maximum value, when the peripheral angular displacement is held constant, is larger for air blown bitumen than blended bitumen with the PDA pitch being in between blended and air blown bitumen. Figure 8 plots the variation of the normal force with time for the three samples. We again find that PDA pitch requires the maximum normal force to maintain the gap between the plates, but it decays faster than air blown bitumen (see Fig. 9). This marked difference in the response of PDA pitch in comparison to bitumen is seen not only with unaged samples (shown in Figs. 6 through 9) but also with aged samples (not shown). As one would expect, these observations do not depend on the angular velocity of the top plate.

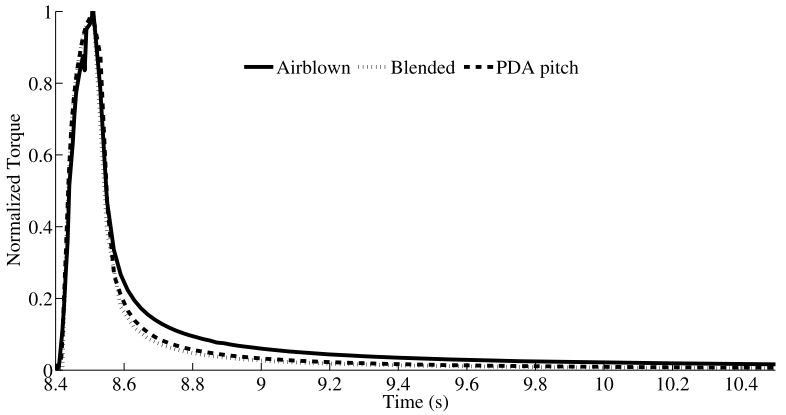

Fig. 7 Variation of normalized torque with time for unaged specimens tested at a maximum angular velocity of 0.625 rad/s. Only the third cycle is shown

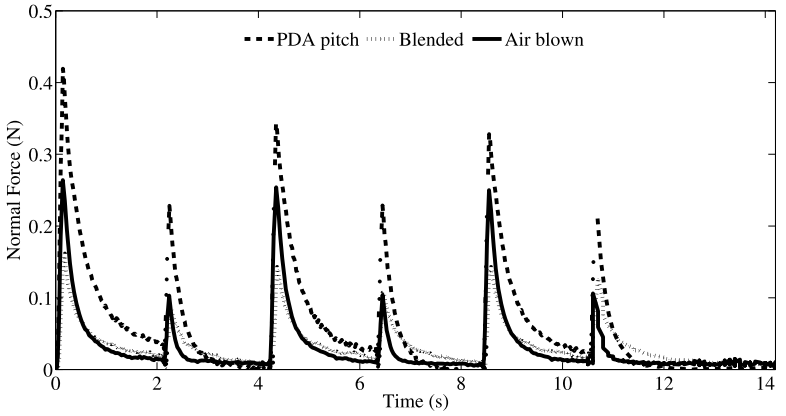

Fig. 8 Variation of normal force with time for unaged specimens tested at a maximum angular velocity of 0.625 rad/s

Before we continue with the discussion of the influence of aging on the rheology of the bitumen samples tested here, a few clarifications related to the aging protocols followed for bituminous binders used are in order here. The current aging protocols followed are single-point measurements at some instant on the oxidation time scale. To aid in the accelerated aging of the binders, the temperatures used are considerably higher than the actual pavement temperatures. One of the main issues related to aging is the variation of the properties of bitumen with the time and temperature scale. It is quite doubtful whether these protocols in vogue can give us such a kind of information. Ideally, these aging tests should be run at a series of different temperatures before any quantification can be made. Based on a considerable amount of experimental work on oxidation kinetics, it is seen that the increase of the Newtonian viscosity is a hyperbolic function of oxidation time, and the limiting viscosity associated with this oxidation depends to a large extent on the temperature used for oxidation. More details related to this can be found in Petersen (2009). With the help of Figs. 10 through 15 we try to understand the effect of aging on the three samples being

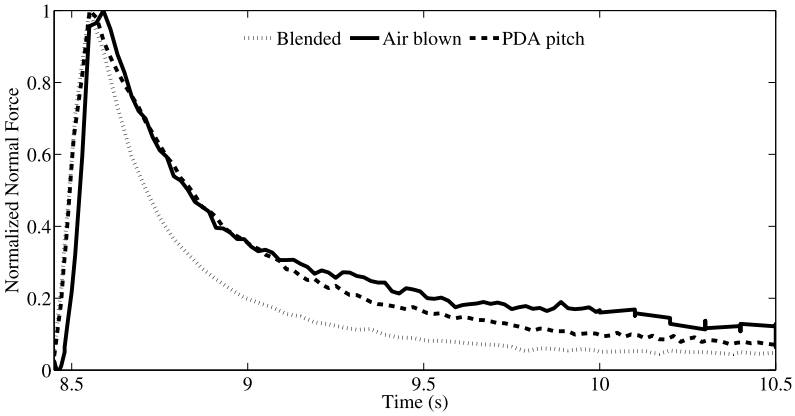

Fig. 9 Variation of normalized normal force with time for unaged specimens tested at a maximum angular velocity of 0.625 rad/s. Only the third cycle is shown

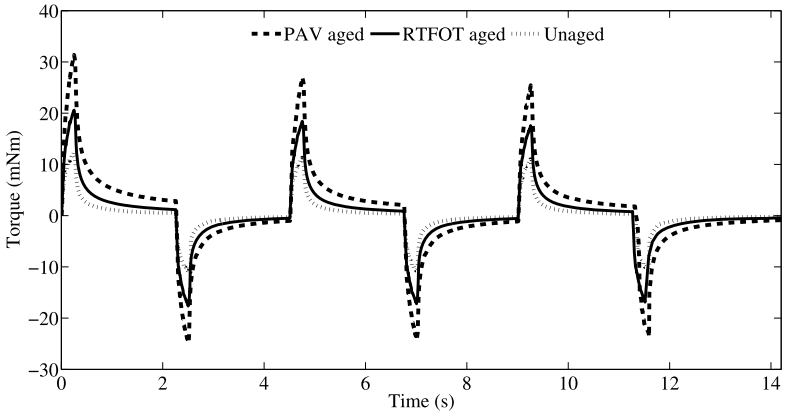

Fig. 10 Variation of torque with time for air blown bitumen samples tested at a maximum angular velocity of 0.25 rad/s under different aging conditions

studied here. It can be seen from Fig. 10 that the torque required to realize a given deformation history increases due to aging. The long-term aged specimens require more torque than short-term aged specimens with the unaged specimens requiring the least torque. Though we have shown this only for air blown bitumen (see Fig. 10) the same is true for the blended case and PDA pitch too (not shown). Even the time taken by the torque to decrease to say 80 percent of its maximum value changes with aging. While for air blown and blended bitumen (see Figs. 11 and 12) the time taken by the torque to decay increases with aging; for PDA pitch (see Fig. 13) short-term aging does not cause a significant difference in the relaxation characteristic of the torque. This may be due to the fact that during the manufacturing process, the oxygen uptake corresponding to short-term aging is satisfied for this material and hence the material may not show a distinct difference.

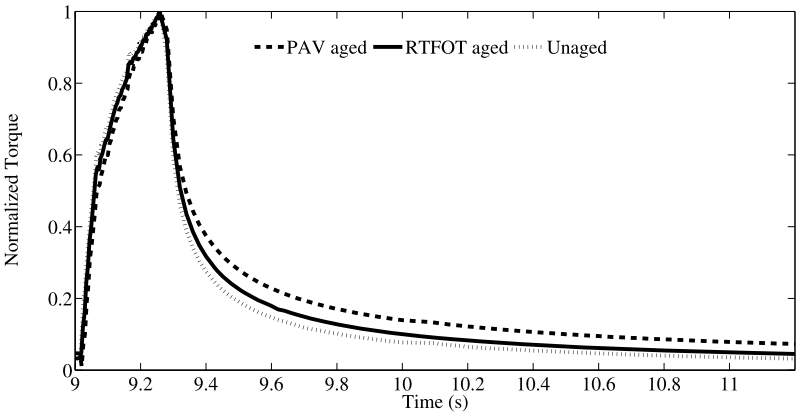

Fig. 11 Variation of normalized torque with time for air blown bitumen samples tested at a maximum angular velocity of 0.25 rad/s under different aging conditions. Only the third cycle is shown

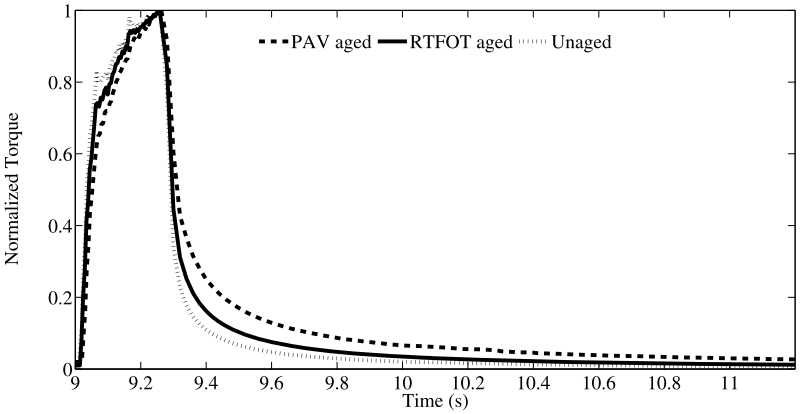

Fig. 12 Variation of normalized torque with time for blended bitumen samples tested at a maximum angular velocity of 0.25 rad/s under different aging conditions. Only the third cycle is shown

In Fig. 14 we plot the variation of the normal force with time for unaged, short-term aged and long-term aged air blown bitumen. As in the case of the torque, the long-term aged specimens require more normal force than the short-term aged specimens with the unaged specimens requiring the least normal force. Though not shown here, we observe the same for blended bitumen and PDA pitch. Examining the normalized normal force (Fig. 15), we find that the time taken by the normal force to decrease by say 40 percent increases with aging. The long-term aged specimens take more time than short-term aged specimens, with the unaged specimens being somewhere inbetween the long-term and short-term aged specimens. This observation seems to hold for both blended and PDA pitch, unlike in the case of torque. Though we concluded all this when the maximum angular velocity of the top plate is 0.25 rad/s, the same holds when the angular velocity is 0.625 rad/s as well.

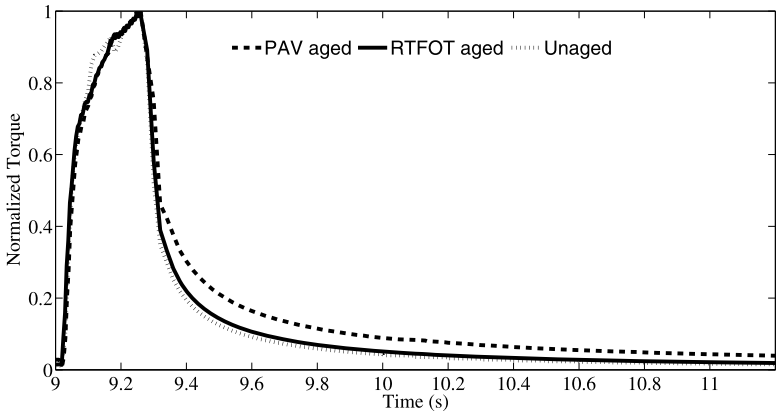

Fig. 13 Variation of normalized torque with time for PDA pitch samples tested at a maximum angular velocity of 0.25 rad/s under different aging conditions. Only the third cycle is shown

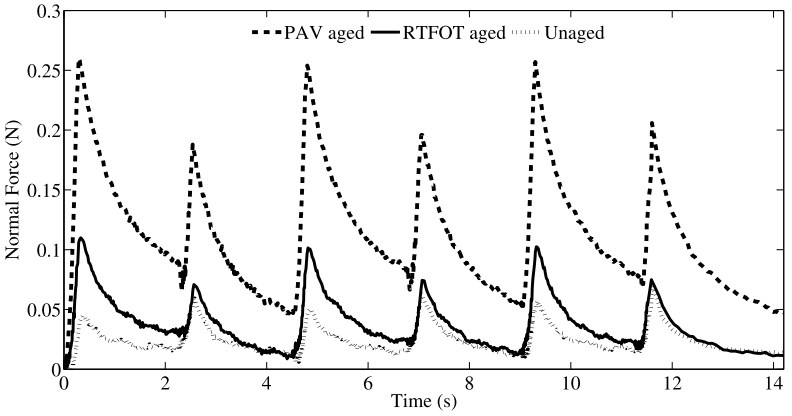

Fig. 14 Variation of normal force with time for air blown bitumen samples tested at a maximum angular velocity of 0.25 rad/s under different aging conditions

3 Constitutive model for bitumen

Since bitumen behaves like an incompressible material, the Cauchy stress tensor $\boldsymbol{\sigma}$ can be decomposed as

$$\boldsymbol{\sigma} = -p\mathbf{1} + \boldsymbol{\tau}, \tag{2}$$

where p is the Lagrange multiplier and $\boldsymbol{\tau}$ is the extra stress. Since differential constitutive relations are simpler to use for capturing normal stress effects (Carreau et al. 1997), we chose to model the bitumen using a differential type constitutive relations. We explore the possibility of modeling bitumen using an implicit constitutive relation for extra stress, of the following form:

$$\hat{\mathbf{f}}\big(\mathbf{d}, \boldsymbol{\tau}, \overset{\nabla}{\boldsymbol{\tau}}\big) = \mathbf{0}, \tag{3}$$

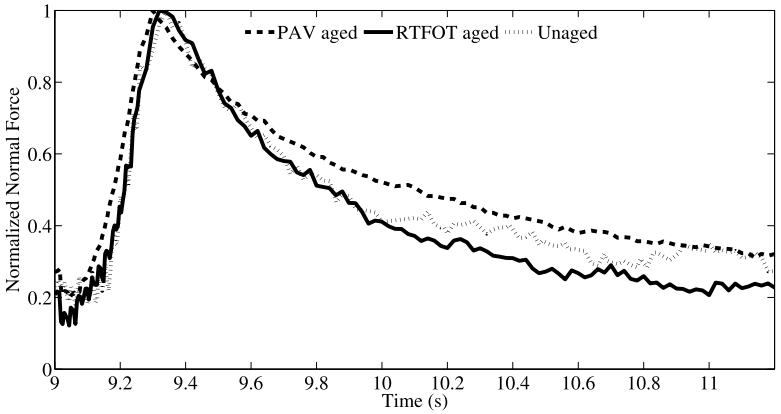

Fig. 15 Variation of normalized normal force with time for air blown bitumen samples tested at a maximum angular velocity of 0.25 rad/s under different aging conditions. Only the third cycle is shown

where $\overset{\nabla}{\boldsymbol{\tau}} = \frac{D\boldsymbol{\tau}}{Dt} - \mathbf{l}\boldsymbol{\tau} - \boldsymbol{\tau}\mathbf{l}^t$, $\mathbf{d} = \frac{1}{2}[\mathbf{l} + \mathbf{l}^t]$, $\mathbf{l} = \text{grad}(\mathbf{v})$. Here $\mathbf{l}$ is the Eulerian velocity gradient, and $\frac{D(\cdot)}{Dt}$ stands for the total time derivative and $\overset{\nabla}{(\cdot)}$ denotes the Oldroyd derivative (Oldroyd 1950). As we require that the constitutive relation satisfy the restriction due to material objectivity (see Carreau et al. 1997), we have used an objective rate, specifically, the Oldroyd derivative. Further, we have restricted ourselves to a class of models that involve only the first temporal derivative of the extra stress. This is because, if higher order temporal derivatives of stress are involved, specifying the initial conditions becomes an issue while solving initial-boundary value problems, and hence we attempted to model the response of the bitumen without using higher order temporal derivatives of stress. It is possible that by using a different objective rate and/or higher order temporal derivatives of the stress, the same response of the bitumen could also be captured.

Material objectivity requires that the function $\hat{\mathbf{f}}$ be isotropic. Then one can obtain a general representation for this isotropic function $\hat{\mathbf{f}}$, following the work of Spencer (1971). Specializing this general expression for the bitumen sample tested here, we find that it is sufficient to consider a constitutive relation of the form

$$\boldsymbol{\tau} + \lambda_1 \overset{\nabla}{\boldsymbol{\tau}} + \lambda_2 \frac{tr(\overset{\nabla}{\boldsymbol{\tau}}\mathbf{d})}{tr(\mathbf{d}^2)}\mathbf{d} + \lambda_3 \frac{tr(\boldsymbol{\tau}\mathbf{d})}{tr(\mathbf{d}^2)}\mathbf{d}^2 = \eta\mathbf{d}, \tag{4}$$

where η, λ_1, λ_2, and λ_3 are constants.

The model is constructed so that the shear stresses and normal stresses have different relaxation times. We should clarify that the material possessing different relaxation times for normal and shear stresses does not mean that it is anisotropic. It would be anisotropic only if the normal and/or shear stresses acting along different planes have different relaxation times. It is possible that some other specification of the material response functions also would be able to capture the response of the bitumens tested.

By virtue of the material having different relaxation times for the normal and shear stresses, different motions, for example uniaxial extension and shear, will have different relaxation times which the present model is capable of predicting. Of interest, here, is a displacement controlled experiment in which the specimen is uniaxially extended along the x direction, held for some time less than its relaxation time, and then brought back to its

original length and then sheared in the xy plane without giving time for the specimen to relax and come to a zero stress state after uniaxial extension. The model (4) predicts that the relaxation time changes abruptly when the motion changes. Whether this happens in experiments is not known, as we are not aware of such experimental data or a set-up where this described motion or similar motion field can be achieved.

As will become evident in Sect. 4.6, λ_1 represents the relaxation time of the axial load (normal stress), $\lambda_1 + \lambda_2$ represents the relaxation time of the torque (shear stress). Similarly, and while η predominantly determines the value of the torque obtained for the shear rate, λ_3 determines the value of the axial load realized for a given shear rate. One would expect that the second law of thermodynamics places some restrictions on the material parameters. However, for non-linear implicit constitutive relations of the kind being studied here, it is not possible to integrate and obtain the Cauchy stress to enable enforcement of the second law of thermodynamics. Recently, Rajagopal and Srinivasa (2011) observed that if one uses the Gibbs potential as the primary state function one can easily develop implicit constitutive relations that are consistent with the second law of thermodynamics. At present their framework does not account for the material response functions being a function of $\overset{\triangledown}{\boldsymbol{\tau}}$, but we found that allowing this dependence enables one to easily capture the difference in the relaxation times of the normal stresses and the shear stresses.

4 Formulation and solution of the boundary value problem

In this section, we formulate and solve the boundary value problem corresponding to that of the experimental set-up for the constitutive relation given in (4).

4.1 Geometry

Here we are interested in the response of bitumen which occupies the region between two parallel concentric plates with its sides open to atmospheric pressure. Thus, mathematically the bitumen is said to occupy the region:

$$\mathcal{B} = \left\{(\rho, \vartheta, \xi) | 0 \leq \rho \leq R_o, 0 \leq \vartheta \leq 2\pi, 0 \leq \xi \leq h\right\}, \tag{5}$$

where (ρ, ϑ, ξ) denote the cylindrical polar coordinates of a point and R_o and h are constants with R_o denoting the radius of the cylinder and h the height of the cylinder. For the experiments conducted in this investigation, $R_o = 4$ mm and $h = 1$ mm.

4.2 Motion field and boundary conditions

In this study, we assume that the cylindrically shaped bitumen specimen is subjected to motion:

$$r = R, \qquad \theta = \Theta + \Omega(t)Z, \qquad z = Z, \tag{6}$$

where (R, Θ, Z) are the cylindrical polar coordinates of a typical particle in the reference configuration and (r, θ, z) are the cylindrical polar coordinates of the same particle in the current configuration; $\Omega(\cdot)$ is a function of time. Thus, the particles are subjected to a velocity field

$$\mathbf{v} = RZ\frac{d\Omega}{dt}\mathbf{e}_\theta, \tag{7}$$

where $\mathbf{e}_\theta$ is the circumferential cylindrical polar basis vector in the current configuration. The motion field assumed is consistent with the experimental set-up in that the bottom plate is stationary while the upper plate rotates at an angular speed of $h\frac{d\Omega}{dt}$.

As regards the traction boundary condition, the outer surface of bitumen is free from traction, i.e.,

$$\mathbf{t}_{\mathbf{e}_r}(R_o,\theta,z) = \sigma_{rr}(R_o)\mathbf{e}_r + \sigma_{r\theta}(R_o)\mathbf{e}_\theta + \sigma_{rz}(R_o)\mathbf{e}_z = \mathbf{0}, \tag{8}$$

and the top and bottom surfaces of the cylinder are subjected to an axial force and a torsional moment, i.e.,

$$\int_0^{2\pi}\left(\int_0^{R_o}\mathbf{t}_{\mathbf{e}_z}(r,\theta,0)\,dr\right)d\theta = \int_0^{2\pi}\left(\int_0^{R_o}\mathbf{t}_{\mathbf{e}_z}(r,\theta,h)\,dr\right)d\theta = \mathcal{L}\mathbf{e}_z,$$

$$\int_0^{2\pi}\left(\int_0^{R_o}\mathbf{t}_{\mathbf{e}_z}(r,\theta,0)\wedge\mathbf{e}_r r\,dr\right)d\theta = \int_0^{2\pi}\left(\int_0^{R_o}\mathbf{t}_{\mathbf{e}_z}(r,\theta,h)\wedge\mathbf{e}_r r\,dr\right)d\theta = \mathcal{T}\mathbf{e}_z,$$

where

$$\mathbf{t}_{\mathbf{e}_z} = \sigma_{rz}\mathbf{e}_r + \sigma_{\theta z}\mathbf{e}_\theta + \sigma_{zz}\mathbf{e}_z \tag{9}$$

and $\mathbf{a}\wedge\mathbf{b}$ denotes the cross product between vectors $\mathbf{a}$ and $\mathbf{b}$.

Before proceeding, a few comments on the assumed motion field (6) are in order. Since the work of Berker (1979) for Navier–Stokes fluids, it is known that flows that are not axially symmetric are possible in this geometry. However, Berker (1979) considered the case of parallel disks rotating about a common axis with the same angular speed, in other words, a rigid body motion. Parter and Rajagopal (1984) investigated the problem of flow of the classical linearly viscous fluid between parallel disks rotating about a common axis with differing angular speeds, and they showed that the solutions lack axial symmetry. Huilgol and Rajagopal (1987) investigated the same problem for an Oldroyd-B fluid and showed that four functions of the axial coordinate determine the non-axisymmetric velocity fields. For viscoelastic fluids too, it is known (Jackson et al. 1984; Larson 1992; Mckinley et al. 1991) that secondary flows arise in this geometry. Further it is known that these secondary flows dominate the flow field when the angular velocity of the top plate ($h\frac{d\Omega}{dt}$) and the shear rate ($R\frac{d\Omega}{dt}$) exceed a critical value, which depends on the material being tested. The reader is referred to Rajagopal (1992) for a detailed review of the issues related to symmetric and asymmetric solutions for both the classical linearly viscous fluid and viscoelastic fluids between rotating disks.

Many of the theoretical (Phan-Thien 1983; Walsh 1987; Ji et al. 1990; Crewther et al. 1991; Öztekin and Brown 1993) as well as experimental (Magda and Larson 1988; Mckinley et al. 1991) investigations have been carried out on Oldroyd-B, Boger fluids and Phan–Thien–Tanner fluids. These fluids are characterized by a single relaxation time for both the normal and shear stresses. However, for the fluid tested here, there are two relaxation times—one for the shear stress and one for the normal stress. Thus, an analysis is required to find the critical value of the angular velocity for a given geometry of the rheometer as to when these secondary flows will dominate the flow field. Despite this, we observe that, since in this study the maximum angular velocity that the top plate is subjected to is less (0.625 rad/s), we did not observe secondary flows and hence the assumed motion field (6) is reasonable.

Also, we examined if the present material undergoes edge fracture, a phenomenon first reported by Hutton (1969) for highly elastic polymeric melts, but we observed none. Tanner and Keentok (1983) conjectured that when axial loads exceed a particular value, edge

fracture occurs and later Lee et al. (1992) experimentally verified the same conjecture in a cone and plate geometry. Even though we measured axial loads, their magnitudes are less than 0.5 N and it appears that they did not exceed the critical value required to cause edge fracture, justifying the assumed motion field (6). However, analysis is required to mathematically establish this for the present model.

4.3 Kinematics

The cylindrical polar matrix components of the gradient of velocity with respect to the current coordinates for the velocity field (7) are calculated by

$$\mathbf{l} = \begin{pmatrix} \frac{\partial v_r}{\partial r} & \frac{1}{r}\frac{\partial v_r}{\partial \theta} - \frac{v_\theta}{r} & \frac{\partial v_r}{\partial z} \\ \frac{\partial v_\theta}{\partial r} & \frac{1}{r}\frac{\partial v_\theta}{\partial \theta} + \frac{v_r}{r} & \frac{\partial v_\theta}{\partial z} \\ \frac{\partial v_z}{\partial r} & \frac{1}{r}\frac{\partial v_z}{\partial \theta} & \frac{\partial v_z}{\partial z} \end{pmatrix} = \begin{pmatrix} 0 & -Z\frac{d\Omega}{dt} & 0 \\ Z\frac{d\Omega}{dt} & 0 & R\frac{d\Omega}{dt} \\ 0 & 0 & 0 \end{pmatrix}. \tag{10}$$

The symmetric part of the velocity gradient is then computed as

$$\mathbf{d} = \begin{pmatrix} 0 & 0 & 0 \\ 0 & 0 & \frac{R}{2}\frac{d\Omega}{dt} \\ 0 & \frac{R}{2}\frac{d\Omega}{dt} & 0 \end{pmatrix}. \tag{11}$$

It could immediately be verified that the condition of incompressibility, $\operatorname{div}(\mathbf{v}) = 0$, is trivially satisfied for the assumed motion field (6).

4.4 Equilibrium equations

Since the experiments performed are at low angular velocities, the contribution of the inertial terms in the equilibrium equations is neglected along with the body forces. Since the velocity gradient is a function of only R and t, it follows from the constitutive relation given by (4) that the extra stress also depends only on R (or r, since $r = R$) and t.

Consequently, the equilibrium equations $\operatorname{div}(\boldsymbol{\sigma}) = \mathbf{0}$ reduce to

$$-\frac{\partial p}{\partial R} + \frac{\partial \tau_{rr}}{\partial R} + \frac{\tau_{rr} - \tau_{\theta\theta}}{R} = 0, \tag{12}$$

$$\frac{\partial \tau_{r\theta}}{\partial R} - \frac{\partial p}{\partial \theta} + \frac{2}{R}\tau_{r\theta} = 0, \tag{13}$$

$$\frac{\partial \tau_{rz}}{\partial R} - \frac{\partial p}{\partial z} + \frac{\tau_{rz}}{R} = 0. \tag{14}$$

Integrating (12) through (14) along with the boundary conditions (8), we obtain

$$\tau_{r\theta}(R,t) = \tau_{rz}(R,t) = 0, \tag{15}$$

$$\hat{p}(R,t) = \tau_{rr}(R,t) + \int_R^{R_o} \frac{\tau_{rr}(R,t) - \tau_{\theta\theta}(R,t)}{R}\, dR. \tag{16}$$

To relate the Lagrange multiplier with the motion field, the constitutive relation (4) has to be integrated with respect to time, to find the stress components τ_{rr} and $\tau_{\theta\theta}$ as a function of R and time t, which we elaborate on in the next section.

Next, we record the relationship between the torque applied on the rotating plate, ($\mathcal{T}$) and $\tau_{\theta z}(R,t)$:

$$\mathcal{T}(t) = 2\pi \int_{r_i}^{r_o} \tau_{\theta z} r^2 \, dr. \tag{17}$$

Similarly, the applied axial force, $\mathcal{L}$ on the plate to maintain the gap between the plates is computed as

$$\mathcal{L}(t) = 2\pi \int_{r_i}^{r_o} \sigma_{zz} r \, dr. \tag{18}$$

However, when the stresses depend only on r, then the above general expression for axial load reduces to (see Truesdell and Noll 1965)

$$\mathcal{L}(t) = \pi \int_{r_i}^{r_o} (2\tau_{zz} - \tau_{rr} - \tau_{\theta\theta}) r dr + \pi \left(r_o^2 \sigma_{rr}(r_o) - r_i^2 \sigma_{rr}(r_i) \right), \tag{19}$$

which gets further simplified to

$$\mathcal{L}(t) = \pi \int_{R_i}^{R_o} (2\tau_{zz} - \tau_{rr} - \tau_{\theta\theta}) R dR - \pi r_i^2 \sigma_{rr}(r_i), \tag{20}$$

for the assumed boundary conditions (8).

4.5 Kinetics

Based on the traction boundary conditions and the equilibrium equations presented above, the matrix representation for the extra stress is

$$\boldsymbol{\tau} = \begin{pmatrix} \tau_{rr}(R,t) & 0 & 0 \\ 0 & \tau_{\theta\theta}(R,t) & \tau_{z\theta}(R,t) \\ 0 & \tau_{z\theta}(R,t) & \tau_{zz}(R,t) \end{pmatrix}. \tag{21}$$

Consequently, the Lagrangian time derivative of the extra stress for the assumed motion field (6) is

$$\frac{D\boldsymbol{\tau}}{Dt} = \begin{pmatrix} \frac{\partial \tau_{rr}}{\partial t} & (\tau_{rr} - \tau_{\theta\theta}) \frac{d\Omega}{dt} Z & -\tau_{z\theta} Z \frac{d\Omega}{dt} \\ (\tau_{rr} - \tau_{\theta\theta}) \frac{d\Omega}{dt} Z & \frac{\partial \tau_{\theta\theta}}{\partial t} & \frac{\partial \tau_{z\theta}}{\partial t} \\ -\tau_{z\theta} Z \frac{d\Omega}{dt} & \frac{\partial \tau_{z\theta}}{\partial t} & \frac{\partial \tau_{zz}}{\partial t} \end{pmatrix}, \tag{22}$$

and hence the Oldroyd derivative of the extra stress is computed to be

$$\overset{\nabla}{\boldsymbol{\tau}} = \begin{pmatrix} \frac{\partial \tau_{rr}}{\partial t} & 0 & 0 \\ 0 & \frac{\partial \tau_{\theta\theta}}{\partial t} - 2\tau_{z\theta} R \frac{d\Omega}{dt} & \frac{\partial \tau_{z\theta}}{\partial t} - \tau_{zz} R \frac{d\Omega}{dt} \\ 0 & \frac{\partial \tau_{z\theta}}{\partial t} - \tau_{zz} R \frac{d\Omega}{dt} & \frac{\partial \tau_{zz}}{\partial t} \end{pmatrix}. \tag{23}$$

4.6 Governing differential equation

Substituting (11), (21), and (23) into the constitutive relation given in (4) and rearranging we get

$$\tau_{rr} + \lambda_1 \frac{\partial \tau_{rr}}{\partial t} = 0, \tag{24}$$

$$\tau_{\theta\theta} + \lambda_1 \frac{\partial \tau_{\theta\theta}}{\partial t} + \left[\frac{\lambda_3}{2} - 2\lambda_1\right]\tau_{\theta z} R \frac{d\Omega}{dt} = 0, \tag{25}$$

$$\tau_{\theta z} + (\lambda_1 + \lambda_2)\frac{\partial \tau_{\theta z}}{\partial t} - (\lambda_1 + \lambda_2)\tau_{zz} R \frac{d\Omega}{dt} = \frac{R\eta}{2}\frac{d\Omega}{dt}, \tag{26}$$

$$\tau_{zz} + \lambda_1 \frac{\partial \tau_{zz}}{\partial t} + \lambda_3 \tau_{\theta z} R \frac{d\Omega}{dt} = 0. \tag{27}$$

Here the above four first order differential equations in time are solved to obtain τ_{rr}, $\tau_{\theta\theta}$, $\tau_{\theta z}$, and τ_{zz} given the angular velocity of the top plate, which is $\frac{d\Omega}{dt}$, since $h = 1$ mm. These being first order differential equations in time, we need to specify their initial condition. Since the experiments began from quiescent conditions, we require that

$$\tau_{rr}(R, 0) = \tau_{\theta\theta}(R, 0) = \tau_{\theta z}(R, 0) = \tau_{zz}(R, 0) = 0. \tag{28}$$

Integrating (24) along with the initial condition given in (28) we obtain

$$\tau_{rr}(R, t) = 0. \tag{29}$$

It is clear from (24) through (27), that while the relaxation time for the normal stresses is λ_1, for the shear stress, $\tau_{\theta z}$, it is $\lambda_1 + \lambda_2$. As is evident from the experimental data, the relaxation time for the axial load is different from that of the torque, and hence comes the need for these class of models.

4.7 Numerical solution of the governing equation

The remaining three first order coupled differential equations (25) through (27) along with the initial condition given by equation (28) is solved numerically using the built-in ordinary differential equation solver, *ODE45* in MATLAB. This solver computes $\mathbf{y}$ at various values of the independent variable, t, over the domain $0 \le t \le t_o$, such that it satisfies the differential equation of the form $\frac{d\mathbf{y}}{dt} = \mathbf{f}(t, \mathbf{y})$ and the initial condition $\mathbf{y}(0) = \mathbf{y}_o$.

In order to cast the problem at hand in the required form, let

$$\{\mathbf{y}\} = \begin{Bmatrix} y_1 \\ y_2 \\ y_3 \end{Bmatrix} = \begin{Bmatrix} \tau_{\theta\theta} \\ \tau_{\theta z} \\ \tau_{zz} \end{Bmatrix}. \tag{30}$$

Then, using (25) through (27) we compute

$$\left\{\frac{\partial \mathbf{y}}{\partial t}\right\} = \begin{Bmatrix} \frac{\partial y_1}{\partial t} \\ \frac{\partial y_2}{\partial t} \\ \frac{\partial y_3}{\partial t} \end{Bmatrix} = \begin{Bmatrix} -\frac{1}{\lambda_1}[y_1 + [\frac{\lambda_3}{2} - 2\lambda_1]R\frac{d\Omega}{dt}y_2] \\ \frac{1}{\lambda_1+\lambda_2}[\frac{R\eta}{2}\frac{d\Omega}{dt} + [\lambda_1 + \lambda_2]R\frac{d\Omega}{dt}y_3 - y_2] \\ -\frac{1}{\lambda_1}[y_3 + \lambda_3 R\frac{d\Omega}{dt}y_2] \end{Bmatrix}. \tag{31}$$

Since R enters these equations explicitly, the above differential equations are solved at specific but various values of R, so that we obtain $\mathbf{y}$ as a function of t and R. Having obtained τ_{rr} and $\tau_{\theta\theta}$ as a function of t and R, the Lagrange multiplier is obtained from (16), where the integration is performed using the trapezoidal rule, for each time instant. We find the trapezoidal rule to perform satisfactorily, because we computed the stresses for small increments of R.

Table 2 Material parameters for various tested specimens

Bitumen	Aging condition	λ_1 (s)	λ_2 (s)	λ_3 (s)	η (Pa·s)	$\lambda_1+\lambda_2$ (s)
Air blown	Unaged	0.83	−0.79	−1.01	2,18,505	0.04
	RTFOT aged	1.05	−0.97	−1.25	3,85,100	0.08
	PAV aged	1.25	−1.11	−1.30	7,15,096	0.14
Blended	Unaged	0.68	−0.58	−0.79	2,89,520	0.10
	RTFOT aged	0.87	−0.76	−1.03	4,86,679	0.11
	PAV aged	0.93	−0.86	−1.17	9,63,868	0.07
PDA pitch	Unaged	0.53	−0.45	−0.60	6,82,045	0.08
	RTFOT aged	1.11	−1.06	−1.41	10,88,485	0.05
	PAV aged	1.35	−1.27	−1.60	24,30,757	0.08

5 Estimation of material parameters

We find these material parameters—λ_i's and η—such that they minimize

$$\epsilon = \sqrt{\frac{1}{N}\sum_{i=1}^{N}\left[\mathcal{T}^{\text{theory}}(t_i) - \mathcal{T}^{\text{Exp}}(t_i)\right]^2} + \sqrt{\frac{1}{N}\sum_{i=1}^{N}\left[\mathcal{L}^{\text{theory}}(t_i) - \mathcal{L}^{\text{Exp}}(t_i)\right]^2}, \tag{32}$$

where N is the number of experimental measurements, $\mathcal{T}^{\text{Exp}}$ is the torque and $\mathcal{L}^{\text{Exp}}$ is the axial load obtained from the experiments at time t_i. $\mathcal{T}^{\text{theory}}$ and $\mathcal{L}^{\text{theory}}$ are the torque and axial load, respectively, at time t_i, obtained for the guessed values of the material parameters and the given history of angular velocities of the top plate. The minimization is done using the built-in MATLAB function *fminsearch*, which implements a Nelder–Mead direct search method. Initially the material parameters are varied manually and those values for the material parameter that as a result were found to be in reasonable agreement with that of the experiment are given as the initial guess for the minimization algorithm. Table 2 lists the material parameters for various samples tested as obtained from the minimization procedure. All the simulations were run in the Vega Cluster supercomputing facility available at IIT Madras, India. Each simulation run for every material took a CPU time of about 6 hours.

6 Results and discussion

In Sect. 2, based on the experimental data it is observed that:

1. The torque relaxes faster than the normal force.
2. The torque required to realize a given deformation history is highest for the PDA pitch and lowest for air blown bitumen.
3. The torque required to realize a given deformation history is highest for a long-term aged specimen and lowest for an unaged specimen within a given sample.
4. In unaged specimens, the torque relaxes fastest in the case of air blown bitumen samples and slowest in blended bitumen.
5. While in both the bitumen and PDA pitch the aging causes the torque to relax slower, in short-term aged PDA pitch the difference is insignificant.
6. In unaged specimens, the normal force required to maintain the gap between the plates is highest for PDA pitch and lowest for air blown bitumen.

Table 3 R^2 for various specimens tested under different conditions

Bitumen	Aging condition	$\frac{d\Omega}{dt} = 0.25$rad/s		$\frac{d\Omega}{dt} = 0.625$rad/s	
		Torque	Axial load	Torque	Axial load
Air blown	Unaged	0.95	0.63	0.90	0.65
	RTFOT aged	0.96	0.76	0.91	0.75
	PAV aged	0.93	0.71	0.89	0.57
Blended	Unaged	0.82	0.78	0.84	0.60
	RTFOT aged	0.93	0.62	0.91	0.76
	PAV aged	0.97	0.54	0.83	0.69
PDA pitch	Unaged	0.91	0.71	0.97	0.73
	RTFOT aged	0.93	0.52	0.91	0.76
	PAV aged	0.81	0.70	0.88	0.72

7. The normal force required to maintain the gap between the plates is highest for long-term aged specimens and lowest for unaged specimens.
8. In unaged specimens, the normal force relaxes fastest in blended bitumen and slowest in the case of air blown bitumen.
9. The normal force relaxes slower as the sample is aged for all the three samples tested.

The developed model seems to be consistent with most of these observations. Comparing the values of relaxation time for normal force, λ_1, with the relaxation time for torque, $\lambda_1 + \lambda_2$, it can be seen that $\lambda_1 > (\lambda_1 + \lambda_2)$, and hence we conclude that the torque relaxes faster than the normal force. The magnitude of the torque applied to realize a deformation history depends on the value of η. The variation in the observed value of η is consistent with observations 2 and 3 above. Similarly, the variation in the relaxation time for the torque, $\lambda_1 + \lambda_2$, is consistent with the observations 4 and 5 listed above. The magnitude of the normal force applied to maintain the gap between the parallel plates depends directly on the value of parameter λ_3 and indirectly on η. It can be found from Table 2 that, while being consistent with observation 7, the magnitude of λ_3 values increases with aging, and it is not consistent with observation 6. The reason for this is yet to be understood.

Corresponding to the two protocols performed on each of the specimens, Table 3 lists the R^2 value for the torque and normal force. It can be seen from the table that the fits for the normal force are not as good as the fits for the torque.

Figure 16 shows the predictions for the torque for unaged PDA pitch, and Fig. 17 shows the same for long-term aged PDA pitch. Figure 18 shows the predictions for the normal force for unaged blended bitumen, and Fig. 19 shows the same for short-term aged PDA pitch. These predictions correspond to the best and worst case of the prediction for the normal force with R^2 values of 0.78 and 0.52, respectively.

7 Conclusions

Here we report experimental investigations conducted on blended and air blown bitumen of the same grade, processed from the same crude source. PDA pitch, one of the blending component for blended bitumen was also tested. All these three samples were tested under unaged, short-term aged and long-term aged conditions. Stress relaxation experiments were conducted on each of these nine specimens in a dynamic shear rheometer and the evolution

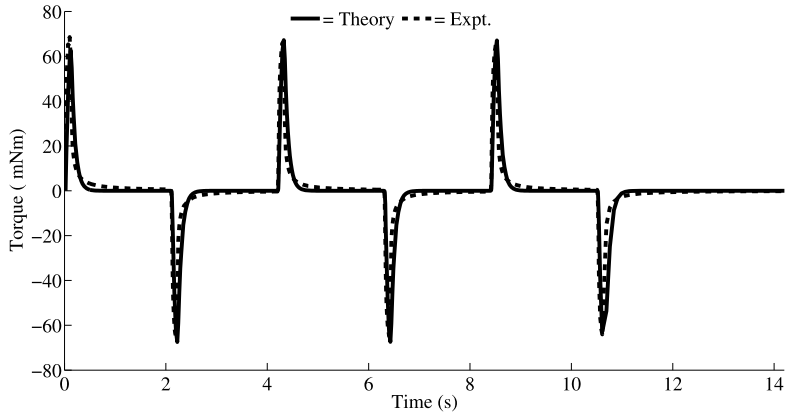

Fig. 16 Comparison of the torque predicted by the model with the experimentally observed values for unaged PDA pitch tested at a maximum angular velocity of 0.625 rad/s

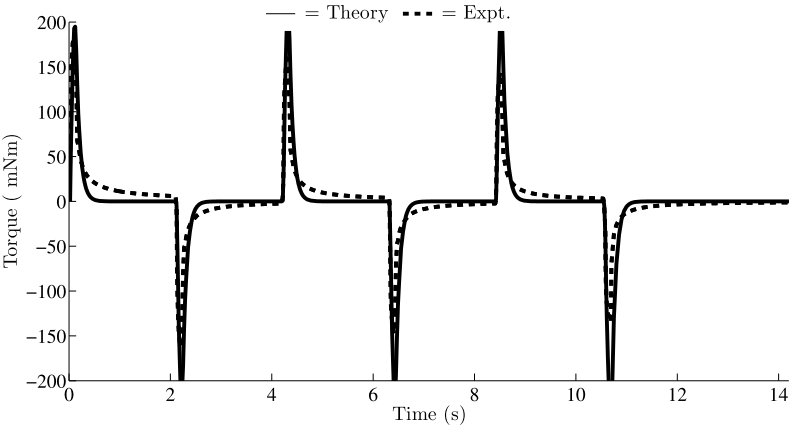

Fig. 17 Comparison of the torque predicted by the model with the experimentally observed values for long-term aged PDA pitch tested at a maximum angular velocity of 0.25 rad/s

of the torque and normal force measured. It is seen that the torque relaxed faster than the normal force for all the material and for all the aging conditions. One of the interesting features seen in the experimental result reported here is that the time at which the maximum torque needs to be applied is different from the time at which the maximum normal force occurs. Comparing the materials tested, it is seen that the torque required is always highest for PDA pitch for a given deformation history. The relaxation mechanism of the material is also influenced by the aging conditions of the material. Aging makes the material stiffer and the relaxation of normal force is slower when compared to the unaged materials. An appropriate frame-invariant model was developed for modeling the response of the tested materials. It is seen from the corroboration of the experimental results with the model simulation that the prediction for the torque is reasonable with R^2 values ranging from 0.81 to 0.96; however, the normal force predictions are slightly poor with the R^2 values ranging from 0.52 to 0.78.

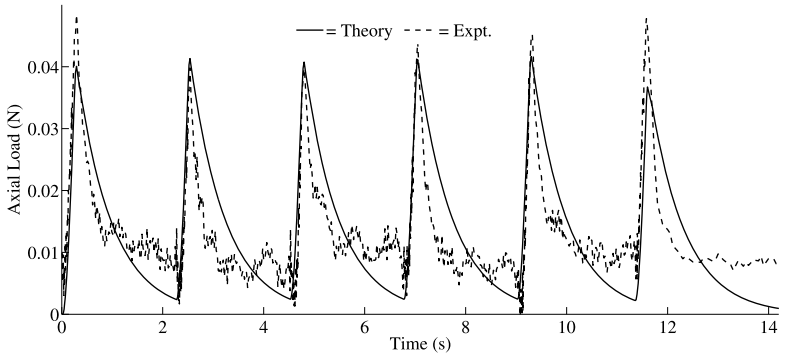

Fig. 18 Comparison of the normal force predicted by the model with the experimentally observed values for unaged blended bitumen tested at a maximum angular velocity of 0.25 rad/s

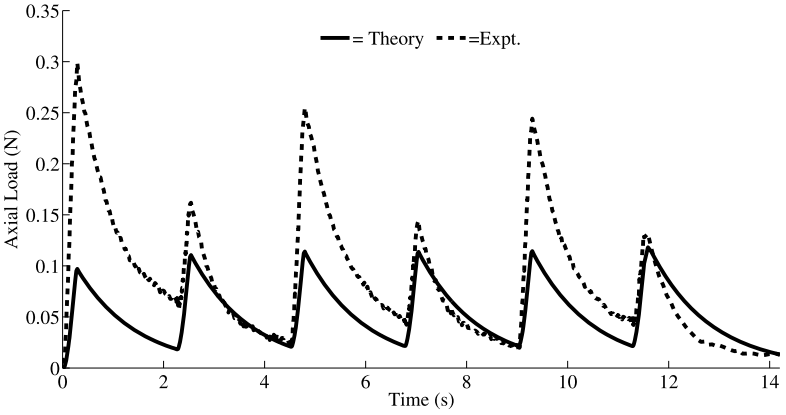

Fig. 19 Comparison of the normal force predicted by the model with the experimentally observed values for short-term aged PDA pitch tested at a maximum angular velocity of 0.25 rad/s

The experimental results reported here are the first of this kind for a variety of bitumens under different aging conditions. The influence of aging, processing method, and blend component (in this case PDA pitch) on the overall rheological behavior of bitumen is studied. One of the missing links in the constitutive modeling studies on bitumen is the change in the rheology of the material during aging, and this study attempts to fill that gap through experiments and appropriate models.

Acknowledgements We thank M/s Chennai Petroleum Corporation Limited, Chennai, India, for processing and providing all the bitumen samples. Dr. Abhijit P Deshpande, Department of Chemical Engineering, IIT Madras is acknowledged here for the stimulating discussion related to the use of the dynamic shear rheometer. High Performance Computing Environment at IIT Madras is gratefully acknowledged for providing us access to the Vega Cluster super computer.

References

ASTM D2872: Standard Test Method for Effect of Heat and Air on a Moving Film of Asphalt (Rolling Thin-Film Oven Test) (2004)

ASTM D3381: Standard Specification for Viscosity-Graded Asphalt Cement for Use in Pavement Construction (2009)
ASTM D5: Standard Test Method for Penetration of Bituminous Materials (2006)
ASTM D6373: Standard Specification for Performance Graded Asphalt Binder (2007)
ASTM D6521: Standard Practice for Accelerated Aging of Asphalt Binder Using a Pressurized Aging Vessel (PAV) (2008)
ASTM D7552: Standard Test Method for Determining the Complex Shear Modulus (G*) Of Bituminous Mixtures Using Dynamic Shear Rheometer (2009)
Attané, P., Soucemarianadin, A., Turrel, G., Prud'Homme, J.B.: Non-linear behaviour of asphalts in steady and transient shear flow. Rheol. Acta **23**(3), 297–310 (1984)
Berker, R.: A new solution of the Navier–Stokes equation for the motion of a fluid contained between two parallel planes rotating about the same axis. Arch. Mech. Stosow. **31**, 265–280 (1979)
BIS: Indian standard paving bitumen—specification (third revision) (2006)
Carreau, P.J., DeKee, D.C.R., Chhabra, R.P.: Rheology of Polymeric Systems—Principals and Applications. Hanser Publications, New York (1997)
Cheung, C.Y., Cebon, D.: Experimental study of pure bitumens in tension, compression, and shear. J. Rheol. **41**(1), 45–74 (1997)
Chockalingam, K., Saravanan, U., Krishnan, J.M.: Characterization of petroleum pitch using steady shear experiments. Int. J. Eng. Sci. **48**(11), 1092–1109 (2010)
Crewther, I., Huilgol, R.R., Jozsa, R.: Axisymmetric and non-axisymmetric flows of a non-Newtonian fluid between coaxial rotating discs. Philos. Trans. R. Soc., Math. Phys. Eng. Sci. **337**(1648), 467–495 (1991). http://www.jstor.org/stable/53978
Dickinson, E.J.: The visco-elastic behavior of confined liquid films in the direction normal to the plane of the film. J. Rheol. **14**(1), 77–81 (1970)
Dickinson, E.J., Witt, H.P.: The visco-elastic behavior of confined thin films of bitumen in tension compression. J. Rheol. **13**(4), 485–511 (1969)
Dobson, G.R.: The dynamic mechanical properties of bitumen. Proc - Assoc Asph. Paving Technol. **38**, 123–139 (1969)
Filograna, L., Racioppi, M., Saccomandi, G., Sgura, I.: A simple model of nonlinear viscoelasticity taking into account stress relaxation. Acta Mech. **204**(1–2), 21–36 (2009). doi:10.1007/s00707-008-0033-7
Fröhlich, H., Sack, R.: Theory of the rheological properties of dispersions. Proc. R. Soc. Lond. Ser. A, Math. Phys. Sci. **185**(1003), 415–430 (1946)
Hatschek, E.: The Viscosity of Liquids. Bell and Sons Limited, London (1928)
Hraiki, S.: Viscoplastic properties of asphaltic bitumen. Rheol. Acta **14**(7), 656–659 (1975). doi:10.1007/BF01520819
Huilgol, R.R., Rajagopal, K.R.: Non-axisymmetric flow of a viscoelastic fluid between rotating disks. J. Non-Newton. Fluid Mech. **23**, 423–434 (1987)
Hutton, J.: Fracture and secondary flow of elastic liquids. Rheol. Acta **8**(1), 54–59 (1969)
Jackson, J.P., Walters, K., Williams, R.: A rheometrical study of Boger fluid. J. Non-Newton. Fluid Mech. **14**, 173–188 (1984)
Ji, Z., Rajagopal, K., Szeri, A.Z.: Multiplicity of solutions in von Karman flows of viscoelastic fluids. J. Non-Newton. Fluid Mech. **36**, 1–25 (1990)
Jongepier, R., Kuilman, B.: The dynamic shear modulus of bitumens as a function of frequency and temperature. Rheol. Acta **9**(1), 102–111 (1970)
Krishnan, J.M., Rajagopal, K.R.: Review of the uses and modeling of bitumen from ancient to modern times. Appl. Mech. Rev. **56**(2), 149–214 (2003)
Krishnan, J.M., Rajagopal, K.R.: On the mechanical behavior of asphalt. Mech. Mater. **37**(11), 1085–1100 (2005)
Larson, R.: Instabilities in viscoelastic flows. Rheol. Acta **31**, 213–263 (1992)
Lee, C., Tripp, B., Magda, J.: Does N_1 or N_2 control the onset of edge fracture? Rheol. Acta **31**, 306–398 (1992)
Lesueur, D.: The colloidal structure of bitumen: consequences on the rheology and on the mechanisms of bitumen modification. Adv. Colloid Interface Sci. **145**(1–2), 42–82 (2009)
Lesueur, D., Gerard, J.F., Claudy, P., Letoffe, J.M., Planche, J.P., Martin, D.: A structure-related model to describe asphalt linear viscoelasticity. J. Rheol. **40**(5), 813–836 (1996)
Lethersich, W.: The mechanical behavior of bitumen. J. Soc. Chem. Ind., Lond. **61**, 101–108 (1942)
Magda, J.J., Larson, R.G.: A transition occurring in ideal elastic liquids during shear flow. J. Non-Newton. Fluid Mech. **30**, 1–19 (1988)
Mckinley, G., Byars, J., Brown, R., Armstrong, G.: Observations on the elastic instability in cone-and-plate and parallel-plate flows of a polyisobutylene Boger fluid. J. Non-Newton. Fluid Mech. **40**, 201–229 (1991)

Newman, J.W.: What is petroleum pitch? In: Deviney, M.L., O'Grady, T.M. (eds.) Petroleum Derived Carbons, ACS Symposium Series, vol. 21, Chap. 5, pp. 52–62. American Chemical Society, Washington (1976)
Oldroyd, J.G.: On the formulation of rheological equations of state. Proc. R. Soc. Lond. Ser. A, Math. Phys. Sci. **200**(1063), 523–541 (1950)
Ossa, EA, Deshpande, V.S., Cebon, D.: Phenomenological model for monotonic and cyclic behavior of pure bitumen. J. Mater. Civ. Eng. **17**(2), 188–197 (2005)
Öztekin, A., Brown, R.: Instability of a viscoelastic fluid between rotating parallel disks: analysis for the oldroyd-b fluid. J. Fluid Mech. **255**, 473–502 (1993)
Parter, S.V., Rajagopal, K.R.: Swirling flow between rotating plates. Arch. Ration. Mech. Anal. **86**, 305–315 (1984)
Petersen, J.C.: A Review of the Fundamentals of Asphalt Oxidation—Chemical, Physicochemical, Physical Property, and Durability Relationships. Transportation Research Circular E-C140. Transportation Research Board, Washington (2009)
Phan-Thien, N.: Coaxial-disk flow of an oldroyd-b fluid: exact solution and stability. J. Non-Newton. Fluid Mech. **13**, 325–340 (1983)
Rajagopal, K.R.: Flow of viscoelastic fluids between rotating disks. Theor. Comput. Fluid Dyn. **3**, 185–206 (1992)
Rajagopal, K.R.: On implicit constitutive theories for fluids. J. Fluid Mech. **550**, 243–249 (2006)
Rajagopal, K.R.: The elasticity of elasticity. Z. Angew. Math. Phys. **58**(2), 309–317 (2007)
Rajagopal, K.R., Srinivasa, A.R.: On the thermodynamics of fluids defined by implicit constitutive relations. Z. Angew. Math. Phys. **59**(4), 715–729 (2008)
Rajagopal, K.R., Srinivasa, A.R.: On a class of non-dissipative materials that are not hyperelastic. Proc. R. Soc., Math. Phys. Eng. Sci. **465**(2102), 493–500 (2009). doi:10.1098/rspa.2008.0319
Rajagopal, K.R., Srinivasa, A.R.: A Gibbs-potential-based formulation for obtaining the response functions for a class of viscoelastic materials. Proc. R. Soc., Math. Phys. Eng. Sci. **467**(2125), 39–58 (2011). http://rspa.royalsocietypublishing.org/content/467/2125/39.full.pdf+html
Rajan, N.K., Selvavathi, V., Sairam, B., Krishnan, J.M.: Rheological characterization of blended paving asphalt. Road Mater. Pavement Des. **9**(Sp. Iss. SI), 67–86 (2008)
Rakow, M.: Petroleum oil refining. In: Totten, G.E., Westbrook, S.R., Shah, R.J. (eds.) Fuels and Lubricants Handbook: Technology, Properties, Performance, and Testing. no. MNL37WCD ASTM Manual Series, Chap 1, pp. 3–30. ASTM International, West Conshohocken (2003)
Spencer, A.: Theory of invariants. In: Eringen, C. (ed.) Continuum Physics, pp. 239–353. Academic Press, New York (1971)
Stastna, J., Zanzotto, L.: Linear response of regular asphalts to external harmonic fields. J. Rheol. **43**(3), 719–734 (1999)
Tanner, R., Keentok, M.: Shear fracture in cone-plate rheometry. J. Rheol. **27**(1), 47–57 (1983)
Truesdell, C., Noll, W.: The nonlinear field theories. In: Handbuch der Physik, vol. III/3. Springer, Berlin (1965)
van der Poel, C.: On the rheology of concentrated dispersions. Rheol. Acta **1**(2), 198–205 (1958)
van der Poel, C.: On the rheology of concentrated dispersions. Rheol. Acta **1**(4), 580–581 (1961)
Vijay, R., Deshpande, A.P., Varughese, S.: Nonlinear rheological modeling of asphalt using White–Metzner model with structural parameter variation based asphaltene structural build-up and breakage. Appl. Rheol. **18**(2), 23214–23228 (2008)
Walsh, W.P.: On the flow of a non-Newtonian fluid between rotating co-axial disks. Z. Angew. Math. Phys. **38**, 495–511 (1987)
Wekumbura, C., Stastna, J., Zanzotto, L.: Stress growth coefficient in polymer modified asphalt. Mater. Struct. **38**(282), 755–760 (2005)
Wekumbura, C., Stastna, J., Zanzotto, L.: Destruction and recovery of internal structure in polymer-modified asphalts. J. Mater. Civ. Eng. **19**(3), 227–232 (2007)